

# Probing the central engine of long gamma-ray bursts and hypernovae with gravitational waves and neutrinos

Yudai Suwa\*

*Department of Physics, School of Science, The University of Tokyo,  
Hongo 7-3-1, Bunkyo-ku, Tokyo 113-0033, Japan and*

*Max-Planck-Institut für Astrophysik, Karl-Schwarzschild-Str. 1, D-85741 Garching, Germany*

Kohta Murase†

*Yukawa Institute for Theoretical Physics, Kyoto University,  
Oiwake-cho, Kitashirakawa, Sakyo-ku, Kyoto, 606-8502, Japan*

(Dated: November 1, 2018)

There are the two common candidates as the viable energy source for the central engine of long gamma-ray bursts (GRBs) and hypernovae (HNe), neutrino annihilation and magnetic fields. We investigate gravitational wave (GW) emission accompanied by these two mechanisms. Especially, we focus on GW signals produced by neutrinos from a hyper-accreting disk around a massive black hole. We show that neutrino-induced GWs are detectable for  $\sim 1$  Mpc events by LISA and  $\sim 100$  Mpc by DECIGO/BBO, if the central engine is powered by neutrinos. The GW signals depend on the viewing angle and they are anti-correlated with neutrino ones. But, simultaneous neutrino detections are also expected, and helpful for diagnosing the explosion mechanism when later electromagnetic observations enable us to identify the source. GW and neutrino observations are potentially useful for probing choked jets that do not produce prompt emission, as well as successful jets. Even in non-detection cases, observations of GWs and neutrinos could lead to profitable implications for the central engine of GRBs and HNe.

PACS numbers: 04.30.-w, 14.60.Lm, 98.70.Rz

## I. INTRODUCTION

Gamma-ray bursts (GRBs) are the most luminous explosions in the universe. The production of GRBs is believed to require that only the small amount of matter is accelerated up to ultrarelativistic speeds and collimated as a jet [1, 2]. The duration of GRBs ranges from  $\sim 10^{-3}$  s to  $\sim 10^3$  s, with a roughly bimodal distribution of long GRBs of  $T \gtrsim 2$  s and short GRBs of  $T \lesssim 2$  s. The geometrically corrected gamma-ray energy of long GRBs is typically  $E_\gamma \sim 10^{50-52}$  ergs [3, 4] (see also [5]), which is much smaller than the isotropic gamma-ray energy  $E_\gamma^{\text{iso}} \sim 10^{52-54}$  ergs. The requirements for the energy budget and time scales suggest that long GRBs involve the formation of a black hole (BH) (e.g., [6]) or magnetars via a catastrophic stellar collapse event. The discovery of supernovae (SNe) associated with GRBs brought us the more direct evidence that GRBs result from a small fraction of massive stars that undergo a catastrophic energy release event towards the end of their evolution [7, 8]. Interestingly, some of the SNe associated with GRBs (e.g., GRB 980425, GRB 060218) showed evidence for broad lines indicating high-velocity ejecta with inferred explosion energy of  $E_{\text{kin}} \sim 10^{52}$  ergs (e.g., [9]), and those energetic SNe are often called hypernovae (HNe). The *central engine* of both GRBs and HNe has to supply such an enormous explosion energy (for reviews, e.g., [10]).

For the class of long GRBs, the commonly discussed candidates are massive stars whose core collapses to a black hole, either directly or after a brief accretion episode, possibly in the course of merging with a companion. This *collapsar* scenario is one of the most widely believed scenarios to explain the huge release of energy in GRBs and HNe [6, 11, 12]. In this scenario, the collapsed iron core of a massive star forms a temporary disk around a few solar mass BH and accretes at a high rate ( $\sim 0.1 - 10 M_\odot \text{ s}^{-1}$ ), which is believed to produce a powerful jet leading to a GRB. The duration of the burst in this scenario can be related to the fall-back time of matter to form a disk or the accretion time of the disk. Possibly, HNe that are brighten by nickel could also be explained by a disk wind, which is subrelativistic with a speed comparable to the escape velocity of the inner disk [12].

Provided a disk and BH form, the greatest uncertainty in the collapsar scenario is the mechanism for converting the disk binding energy or BH rotation energy into directed relativistic outflows. So far, two general mechanisms

---

\*suwa@utap.phys.s.u-tokyo.ac.jp

†kmurase@yukawa.kyoto-u.ac.jp

have been proposed: neutrino annihilation and magnetohydrodynamical (MHD) mechanisms in various kinds. In the former case, neutrino pairs are generated in the hot disk and impact one another with the largest angles along the rotational axis and deposit some fraction of the accretion energy [13, 14, 15, 16, 17, 18, 19]. It should be noted that the efficiency of energy deposition is no greater than  $\sim 1\%$  of the total neutrino emission [20], so that the required neutrino energy is  $E_\nu \sim 10^{53-54}$  ergs in order to achieve the jet energy of  $E_j \sim 10^{52}$  ergs (which should be larger than the gamma-ray radiation energy). One important property of this dense, hot accretion flow is that the density is so high that cooling of the flow is dominated by neutrinos. This accretion flow is called neutrino-dominated accretion flow (NDAF). Although neutrinos can escape the flow more easily than photons, they can also be trapped in the flow and fail to escape before being swallowed by the black hole when the accretion rate becomes very high [13, 14, 15]. The other possible mechanism is a MHD-driven explosion, where two options exist for the energy source: the binding energy of the accretion disk [21, 22] and the rotational energy of the BH through the Blandford & Znajek mechanism [23, 24, 25, 26]. In the former case, the magnetic fields are amplified up to  $\sim 10^{15-16}$  G by rotation via some disk instabilities, leading to a strong outflow. In the latter case, the BH and accretion disk are connected with magnetic field lines and the rotational energy of the BH is extracted via these magnetic field lines. In some versions of the MHD scenario, the extracted energy propagates as the Poynting flux and is probably converted into a matter-dominated form at later stages, so that the efficiency of energy deposition is expected to be higher than that of the neutrino-annihilation mechanism.

Although the various possibilities including the fast rotating magnetar scenario [27, 28, 29, 30, 31] as well as the collapsar scenario have been proposed, there has been no direct evidence for the central engine of GRBs. In this paper, we consider gravitational waves (GWs) as a probe of the jet-producing mechanism of GRBs (see [32, 33] for GWs from jet itself). The difficulty in probing the central engine comes from the fact that most observed properties of GRBs come from electromagnetic signals produced in regions far away from the central engine. On the other hand, GWs and neutrinos can reach us without losing information of physical conditions near the central engine. Especially, we focus on the GW emission generated by anisotropic neutrino emission, and estimate its amplitude which were investigated in the context of massive-star collapse [34, 35, 36, 37, 38, 39] (see also, [40, 41]). The amplitude of this GW emission is governed by the radiated neutrino energy that has to be large enough for the neutrino-annihilation mechanism to work as the central engine of GRB jets. As a result, we can show that neutrino-induced GWs are detectable for  $\sim 1$  Mpc events by LISA and  $\sim 100$  Mpc by DECIGO, if the central engine is powered by neutrinos. The coincident neutrino signals can also be detected by using the Super-Kamiokande detector or recently proposed Mton neutrino detectors such as Hyper-Kamiokande. Possible successful detections combined with later electromagnetic observations can give us important clues to the central engine of long GRBs.

This paper is organized as follows. In §II, we describe the formulation used in this work. The necessary expressions of the GW amplitude is presented. In §III, we give spectra of GWs from NDAF and apply the derived formula to a burst or multiple bursts representing GRBs. We also discuss detectability of GWs and whether we can identify a GW event as the formation of NDAF making a GRB and/or HN. In §IV, the gravitational wave background is also discussed.

## II. GRAVITATIONAL WAVES FROM NDAF

Here we consider the gravitational wave emission from anisotropic neutrino radiation, which is proposed by Epstein [42]. Following the formulation developed by previous works [34, 35, 38], we first derive useful formulae of the GW amplitude for axisymmetric emission of neutrinos.

First, we introduce the two coordinate frames shown in figure 1: the source coordinate frame  $(x', y', z')$  and the observer coordinate frame  $(x, y, z)$ . In these coordinate frames, the  $z'$ -axis is chosen as the symmetry axis of source, while  $z$ -axis is set to a line-of-sight direction. Furthermore, the origin of these two coordinate frames are set to the center of a GRB engine. Thus, the viewing angle denoted by  $\xi$  is given by the angle between the  $z$ -axis and the  $z'$ -axis. For simplicity, we assume that the  $z$ -axis lies in  $(x', z')$ -plane. In this case, the two polarization states of GWs satisfying the transverse-traceless conditions become  $h_+^{\text{TT}} \equiv h_{xx}^{\text{TT}} = -h_{yy}^{\text{TT}}$  and  $h_\times^{\text{TT}} \equiv h_{xy}^{\text{TT}} = h_{yx}^{\text{TT}}$  in the observer coordinate. The geometrical setup shown in Figure 1 yields the following relationship between the two polar coordinate frames  $(\theta, \phi)$  and  $(\theta', \phi')$ :

$$\begin{aligned} \sin \theta' \cos \phi' &= \sin \theta \cos \phi \cos \xi + \cos \theta \sin \xi, \\ \sin \theta' \sin \phi' &= \sin \theta \sin \phi, \\ \cos \theta' &= -\sin \theta \cos \phi \sin \xi + \cos \theta \cos \xi. \end{aligned} \tag{1}$$

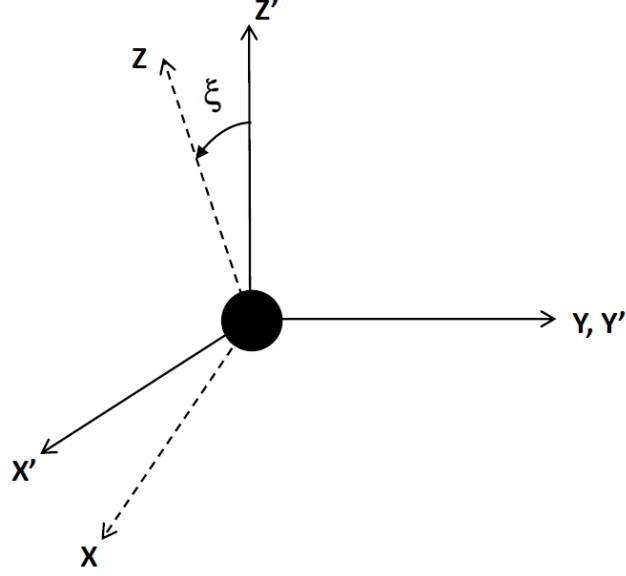


FIG. 1: Source coordinate frame  $(x', y', z')$  and observer coordinate frame  $(x, y, z)$ . The observer resides at a distant point on the  $z$ -axis. The viewing angle is denoted by  $\xi$ , which is the angle between  $z$  and  $z'$  axis. The  $z'$ -axis coincides with the symmetry axis of the source.

With these coordinates, one can obtain the GW amplitude as [35]

$$h_+^{\text{TT}}(t, \xi) = \frac{2G}{c^4 D} \int_{-\infty}^{t-D/c} dt' \int_{4\pi} d\Omega' (1 + \cos \theta) \cos(2\phi) \frac{dL_\nu(\boldsymbol{\Omega}', t')}{d\Omega'}, \quad (2)$$

where  $G$  is the gravitational constant,  $c$  is the speed of light,  $D$  is the distance between the observer and the source, and  $dL_\nu/d\Omega'$  represents the direction-dependent neutrino luminosity per unit of solid angle in the direction of  $\boldsymbol{\Omega}'$ . Note that the counter part of the amplitude,  $h_\times^{\text{TT}}$ , is obtained by replacing  $\cos(2\phi)$  by  $\sin(2\phi)$  in Eq. (2), which vanishes when  $dL_\nu/d\Omega'$  is axially symmetric.

In the above equation,  $\theta$  and  $\phi$  are required to be expressed in terms of the angles  $\theta'$  and  $\phi'$  with respect to the source coordinate variables, and the viewing angle,  $\xi$ . Using Eq. (1), one can obtain the amplitude as following,

$$h_+(t, \xi) = \frac{2G}{c^4 D} \int_{-\infty}^{t-D/c} dt' \int_{4\pi} d\Omega' \Psi(\theta', \phi', \xi) \frac{dL_\nu(\boldsymbol{\Omega}', t')}{d\Omega'}, \quad (3)$$

where  $\Psi(\theta', \phi', \xi)$  denotes the angle dependent factor,

$$\Psi(\theta', \phi', \xi) = (1 + \cos \theta' \cos \xi + \sin \theta' \cos \phi' \sin \xi) \frac{(\sin \theta' \cos \phi' \cos \xi - \cos \theta' \sin \xi)^2 - \sin^2 \theta' \sin^2 \phi'}{(\sin \theta' \cos \phi' \cos \xi - \cos \theta' \sin \xi)^2 + \sin^2 \theta' \sin^2 \phi'}. \quad (4)$$

This is a generalization of the Eqs. (26) and (27) of Müller & Janka [35], who derived the formula for the cases  $\xi = 0$  and  $\pi/2$ , respectively. By integration with respect to the azimuthal angle ( $\phi'$ ) assuming that  $dL_\nu(\boldsymbol{\Omega}', t')/d\Omega'$  is axisymmetric, we obtain

$$h_+(t, \xi) = \frac{2G}{c^4 D} \int_{-\infty}^{t-D/c} dt' \int_0^\pi \sin \theta' d\theta' \Phi(\theta', \xi) \frac{dL_\nu}{d\theta'}(\theta', t'), \quad (5)$$

where

$$\Phi(\theta', \xi) = \begin{cases} -2\pi [1 + \cos \theta' (2 + \cos \xi)] \tan^2 \left( \frac{\xi}{2} \right) & (\text{for } \theta' \geq \xi) \\ -2\pi [1 + \cos \theta' (-2 + \cos \xi)] \cot^2 \left( \frac{\xi}{2} \right) & (\text{for } \theta' < \xi) \end{cases}. \quad (6)$$

When  $\xi = \pi/2$ , the above equations coincide with Eq. (8) of Kotake et al. [38]. With these equations, we estimate the amplitude of gravitational waves. For practical evaluations, we need to know  $dL_\nu(\mathbf{\Omega}, t)/d\Omega$  which should be determined by the nature of the central engine or produced jets. In the following subsections, we regard the shape of NDAF as a geometrically thin disk or an oblate spheroid, by which we obtain the angular dependence of  $dL_\nu(\mathbf{\Omega}, t)/d\Omega$  explicitly.

### A. A geometrically thin disk model

We first consider a geometrically infinitely thin disk as a simple but useful case in order to model NDAF. In this case, the angular dependence of the neutrino emission is written as  $dL_\nu/d\Omega \propto |\cos\theta|$  if we assume that the emission of neutrinos is isotropic at the disk surface. We can write the neutrino luminosity per solid angle as  $dL_\nu/d\theta' = (L_\nu/2\pi)|\cos\theta'|$ , where  $L_\nu$  is the *total* neutrino luminosity.

At first, we consider the case of an observer located in the equatorial plane for simplicity, which means  $\xi = \pi/2$ . In this case Eq.(5) is written as

$$\begin{aligned} h_+(t) &= \frac{2G}{c^4 D} \int_{-\infty}^{t-D/c} dt' \int_0^\pi d\theta' \Phi(\theta') \frac{dL_\nu}{d\Omega'}(\theta', t') \\ &= \frac{2G}{c^4 D} \int_{-\infty}^{t-D/c} dt' L_\nu(t') \int_0^\pi d\theta' (-1 + 2|\cos\theta'|) \sin\theta' |\cos\theta'| \\ &= \frac{2G}{c^4 D} \left(\frac{1}{3}\right) \int_{-\infty}^{t-D/c} L_\nu(t') dt'. \end{aligned} \quad (7)$$

It is worthwhile to note that the anisotropy parameter  $\alpha$  defined by Müller and Janka [35] (see Eq.(29) in their paper) is constant and equal to 1/3 in this case. Since the duration of neutrino emission is finite, the GW amplitude converges to a non-vanishing value[68], which we denote as  $h_\infty$ . With characteristic values, we can write  $h_\infty$  as

$$h_\infty \sim 1.8 \times 10^{-21} \left(\frac{10\text{Mpc}}{D}\right) \left(\frac{E_\nu}{10^{54}\text{ergs}}\right), \quad (8)$$

where  $E_\nu \equiv \int_{-\infty}^{\infty} L_\nu(t') dt'$  is the total energy emitted by neutrinos. In this work, we employ  $E_\nu = 10^{54}$  ergs for calculations of the GW amplitude. This is because the required energy for a GRB jet is  $E_j \sim 10^{52}$  ergs [69] and the efficiency of energy conversion is expected to be  $\sim 1\%$  for the neutrino-annihilation mechanism [13]. In addition, the energy released by matter at innermost stable circular orbit (ISCO) is about 40% of its rest-mass energy for an extremely rotating Kerr BH. This corresponds to  $\sim 10^{54}$  ergs for accretion of  $1 M_\odot$ . This value is also consistent with the observational evidence of GRB-HNe association because the explosion energy of HNe is  $\sim 10$  times larger ( $E_{\text{kin}} \sim 10^{52}$  ergs) than that of ordinary core-collapse SNe, which emit  $E_\nu \sim 3 \times 10^{53}$  ergs by neutrinos. If the explosion mechanism of HNe is similar to that of ordinary SNe, in which the explosion energy is provided by absorption and scattering of neutrinos, the total energy emitted by neutrinos must be larger than that of ordinary SNe, and we may expect  $E_\nu \sim 10^{54}$  ergs.

It is useful to see dependence of the GW amplitude on the viewing angle,  $\xi$ . In the thin disk model, Eq.(2) can be integrated analytically, and we have

$$h_\infty(\xi) = \frac{2G}{c^4 D} \frac{1 + 2\cos\xi}{3} \tan^2\left(\frac{\xi}{2}\right) E_\nu. \quad (9)$$

It is obvious that the GW amplitude is the largest when the observer is located in the equatorial plane, whereas the GW vanishes when the observer is located at the pole. This implies important implication, i.e., anti-correlation between GW signals and prompt gamma-ray photons. Prompt photons themselves are highly beamed ( $\sim 1/\Gamma$ ) since they are emitted from ultrarelativistic jets moving with  $\Gamma \sim 10^{2.5}$ . Therefore, it may not be easy to detect prompt photons when we can expect the strong GW emission. Furthermore, there may be the possible population of failed GRBs whose jets do not generate prompt photons since, e.g., jets are choked in the stellar envelope. As discussed in the next section, GW signals would still be useful as a probe of the central engine even in such cases.

### B. An oblate spheroid

We now consider an oblate spheroid in order to mimic the thickness of NDAF. In this case, the neutrino luminosity per solid angle is  $dL_\nu/d\Omega \propto \sqrt{a^2 + (1-a^2)\cos^2\theta}$ , where  $a$  ( $\leq 1$ ) is the ratio between the length of the major and the

minor axes. The gravitational wave amplitude for an observer in the equatorial plane ( $\xi = \pi/2$ ) can be written as

$$h_\infty(a)|_{\xi=\pi/2} = \frac{2G}{c^4 D} \frac{\sqrt{1-a^2}(1+a+4a^2) - 3a^2(1+a)F(a)}{3(1+a)[\sqrt{1-a^2} + a^2F(a)]} E_\nu, \quad (10)$$

$$F(a) = \log \left( \frac{1 + \sqrt{1-a^2}}{a} \right). \quad (11)$$

Fig 2 shows the GW amplitude from spheroid as a function of  $a$  with  $D = 10$  Mpc and  $E_\nu = 10^{54}$  ergs. For spherical emission ( $a = 1$ ), no GW is emitted by neutrinos. The case of the disk height being similar to the disk radius corresponds to  $a \sim 0.5$  that leads a suppression of GW by a factor of 3 compared to the case  $a = 0$ .

In Fig. 3, we show  $h_\infty(\xi, a)$  normalized to its value for  $\xi = \pi/2$  and  $a = 0$ , which is calculated numerically. The amplitude for  $\xi = \pi/4$  and  $a = 0.5$  is  $\sim 0.18h_\infty(\pi/2, 0)$ . It should be noted that the suppression is not so large even if we include both the viewing angle and thickness of the disk, as long as we consider  $a \lesssim 0.5$  and  $\xi \gtrsim \pi/4$ , respectively. It should be noted that the amplitude of GW is anti-correlated with neutrino. The *apparent* luminosity of neutrino shows the largest value for the observer at pole. When we consider the geometrically thin disk that was discussed in previous subsection, neutrinos can not be observed for the observer at the equatorial plane but GW is observable. As for the oblate spheroid, neutrinos are observable from any direction. The detectability of neutrinos will be discussed in the next section.

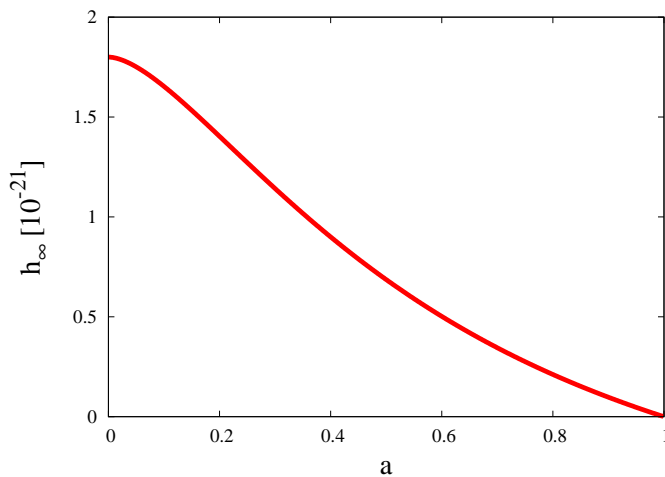


FIG. 2: The GW amplitude from NDAF using an oblate spheroid model as a function of the ratio between the length of the major and the minor axes,  $a$ . We employ  $D = 10$  Mpc and  $E_\nu = 10^{54}$  ergs in this plot. For spherical emission ( $a = 1$ ), no GW are emitted by neutrinos. The case of the disk height being similar to the disk radius corresponds to  $a \sim 0.5$  that leads a suppression of GW by a factor of 3 compared to the case  $a = 0$ .

### III. THE GRAVITATIONAL WAVE SPECTRUM AND APPLICATION TO BURSTS

In this section, we first obtain useful formulae of the GW spectrum from NDAF using the expressions derived in the previous section. We now consider axisymmetric sources, so that the only non-vanishing component is  $h_+$ . As a result, the local energy flux of GWs can be written as

$$\frac{dE_{\text{GW}}}{dAdt} = \frac{c^3}{16\pi G} \left| \frac{d}{dt} h_+(t) \right|^2, \quad (12)$$

where  $dA = D^2 d\Omega$  is the surface element. This is the general expression for the GW flux.

We have calculated the angular dependence of  $dL_\nu(\Omega, t)/d\Omega$  in the previous subsections. Then, we can obtain GW spectra for NDAF mimicked by an infinitely thin disk or an oblate spheroid for given  $L_\nu(t)$ . As an example, let us obtain the useful expression for the case of a geometrically thin disk. (Numerical calculations are required for the

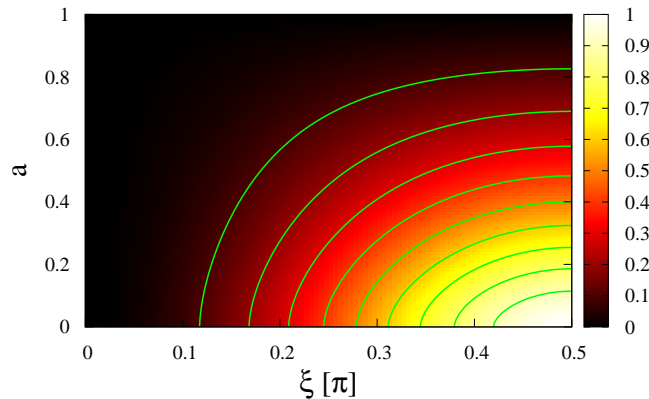


FIG. 3: The GW amplitude from NDAF using an oblate spheroid model as a function of the ratio between the length of the major and the minor axes,  $a$ , and the viewing angle,  $\xi$ , normalized to its value for  $a = 0$  and  $\xi = \pi/2$ .

case of an oblate spheroid.) Let us insert Eq. (7) taking into account the angular dependence by Eq. (9). Then, we get

$$\frac{dE_{\text{GW}}}{dAdt} = \frac{G}{36\pi c^5 D^2} (1 + 2 \cos \xi)^2 \tan^4 \left( \frac{\xi}{2} \right) L_\nu(t)^2. \quad (13)$$

The total energy flowing through  $dA$  between  $t = -\infty$  and  $t = +\infty$  is therefore

$$\frac{dE_{\text{GW}}}{dA} = \frac{G}{36\pi c^5 D^2} (1 + 2 \cos \xi)^2 \tan^4 \left( \frac{\xi}{2} \right) \int_{-\infty}^{\infty} dt L_\nu(t)^2. \quad (14)$$

Integrating over a sphere surrounding the source, we find the total energy emitted by GW as

$$E_{\text{GW}} = \frac{1}{9} \beta \frac{G}{c^5} \int_{-\infty}^{\infty} dt L_\nu(t)^2, \quad (15)$$

where  $\beta = \frac{43}{3} - 20 \ln 2 \sim 0.47039$ . This is consistent with Eq. (31) in Müller & Janka [35] since the anisotropy parameter  $\alpha = 1/3$  in this case as already noted in §II [70]. In order to get a GW spectrum, we write  $L_\nu$  in Eq. (15) in terms of the inverse Fourier transform as

$$L_\nu(t) = \int_{-\infty}^{\infty} \tilde{L}_\nu(f) e^{-2\pi i f t} df. \quad (16)$$

After several algebraic steps, we easily obtain the GW energy spectrum as

$$\frac{dE_{\text{GW}}(f)}{df} = \frac{2}{9} \beta \frac{G}{c^5} |\tilde{L}_\nu(f)|^2, \quad (17)$$

for a geometrically thin disk model for NDAF.

Once we have a GW spectrum  $dE_{\text{GW}}/df$  (obtained numerically or analytically), we can discuss detectability of the GW. For this purpose, we shall use the characteristic GW strain expressed as

$$h_c(f) = \sqrt{\frac{2}{\pi^2} \frac{G}{c^3} \frac{1}{D^2} \frac{dE_{\text{GW}}(f)}{df}} \quad (18)$$

for a given frequency  $f$  [43]. Since we have this characteristic strain  $h_c(f)$  for either model of NDAF (a thin disk or an oblate spheroid), we can also compute signal-to-noise ratios (SNRs) obtained from matched filtering in terrestrial/space gravitational wave experiments. The optimal (with respect to the relative orientation of a source and detector) SNR is given by

$$\text{SNR}^2 = \int_0^\infty d(\ln f) \frac{h_c(f)^2}{h_n(f)^2}, \quad (19)$$

where  $h_n(f) = [5fS_h(f)]^{1/2}$  is the noise amplitude with  $S_h(f)$  being the spectral density of the strain noise in the detector at frequency  $f$ . The factor five refers to averaging over all orientations of the source [43]. This determination of the SNR is optimistic, because a complete set of wave templates required for the matched filtering analysis is not available for burst events. However, SNRs for the other techniques of analysis (e.g., bandpass filtering and noise monitoring in Ref. [43]) can be connected with the SNR obtained from matched filtering within some factors. Thus, Eq. (19) may give a little bit optimistic, but not severely overestimated values.

In the following subsections, we give explicit expressions of  $L_\nu(t)$  in order to apply our formulae to bursts. First, we show GW spectra regarding a GRB as one single burst caused by NDAF, where neutrino emission with  $L_\nu \sim \text{constant}$  is assumed to occur during the duration of the GRB. However, the realistic time dependence of  $L_\nu(t)$  should depend on the nature of the central engine, which is unknown. In fact, the observed complex variability may be one of the clues to the behavior of the central engine. For example, the internal shock model, which is one of the most widely believed scenarios for explaining prompt emission, requires that jets are highly inhomogeneous (i.e., the dispersion of the bulk Lorentz factor should be large). The origin of many subshells moving with different speeds may be or may not be related to the activity of the central engine. In the former case, we may expect that neutrino emission occurs intermittently[71]. This motivates us to consider the case of multiple bursts.

### A. A single burst

In this subsection, we consider a single burst event. We assume the following time evolution of the neutrino luminosity

$$L_\nu(t) = \frac{E_\nu}{T} \Theta(t) \Theta(T - t), \quad (20)$$

where  $T$  is the duration of the central engine of a GRB and  $\Theta$  is the Heaviside step function. This expression corresponds to the case where the neutrino luminosity from NDAF only depends weakly on time during the burst. In this case, the characteristic strain evaluated by Eq. (18) can be written as

$$h_c(f) = \frac{\sqrt{\beta} h_\infty}{\pi^2 T f} |\sin(\pi T f)|, \quad (21)$$

where  $h_\infty$  is the converged value of the GW amplitude obtained by Eq. (8). The spectrum converges to a constant value of  $\sqrt{\beta} h_\infty / \pi$  for  $f \ll 1/T$ . This behavior typically arises from a sudden change of the neutrino luminosity and is called zero-frequency limit of GW memory [44].

Figure 4 shows typical examples of the characteristic strain  $h_c$ . In this figure, the red solid line represents the GW from GRB, which erupts at the center of Galaxy. The green dashed and blue dotted lines show the GW from a source at a distance of 10 Mpc but different durations,  $T = 10$  and 200 s, respectively. The gray dot-dashed line shows the GW from a source with the same parameters as the green dashed line but  $E_\nu = 10^{53}$  ergs. Sensitivity lines for future planned interferometers, that is, advanced-LIGO, LISA, DECIGO/BBO, and ultimate-DECIGO, are also shown in this figure [72]. One can roughly read off the SNR from figure 4. It should be noted that the GW amplitude is larger for the model with  $E_\nu = 10^{53}$  ergs and  $T = 10$  s than one with  $E_\nu = 10^{54}$  ergs and  $T = 200$  s in the range of  $f \gtrsim 0.1$  Hz. Therefore, both the duration and the total energy emitted by neutrinos are important for the discussion of the detectability.

More detailed information of the SNR can be found in figure 5, which gives the SNR for LISA. In this figure, the colored region corresponds to  $\text{SNR} > 1$ . The dotted line is for  $\text{SNR} = 10$ , which is required to detect the GW emission by the burst memory as discussed in Ref. [45]. As the duration becomes longer, the SNR of GWs from GRBs gets smaller. This is because the cutoff frequency, beyond which GW spectra depend on frequency as  $f^{-1}$ , appears at  $f \sim T^{-1}$  so that longer lasting events lead to smaller amplitudes at the high frequency range, whereas amplitudes in the low frequency range are independent of the duration. From this figure, one can see that LISA can detect GW signals up to distances of  $D \sim 1$  Mpc. The same analysis shows that GRBs with distances of  $\sim 100$  Mpc are detectable with DECIGO/BBO as long as the duration  $T \lesssim 10$  s (see figure 6).

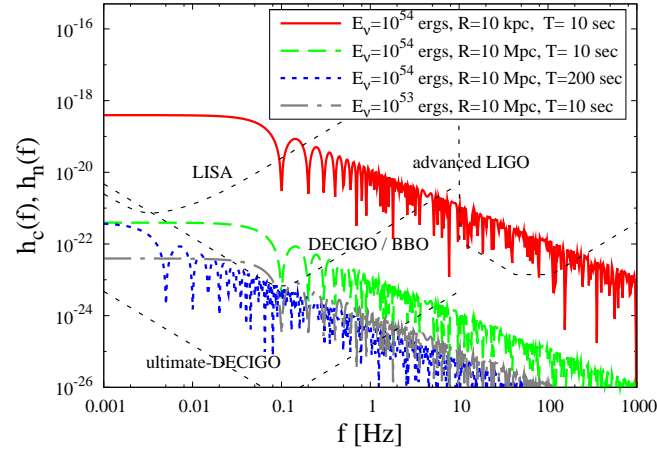


FIG. 4: The characteristic amplitude of GWs from a GRB. Thick lines represent characteristic amplitudes of GW for typical models. The red solid and green dashed lines are for  $T = 10$  s but  $D = 10$  kpc and 10 Mpc, respectively. The blue dotted line is for  $D = 10$  Mpc and  $T = 200$  s. Here, we assume the total energy to be  $E_\nu = 10^{54}$  ergs for red solid, green dashed, and blue dotted lines and  $E_\nu = 10^{53}$  ergs for the gray dot-dashed line.

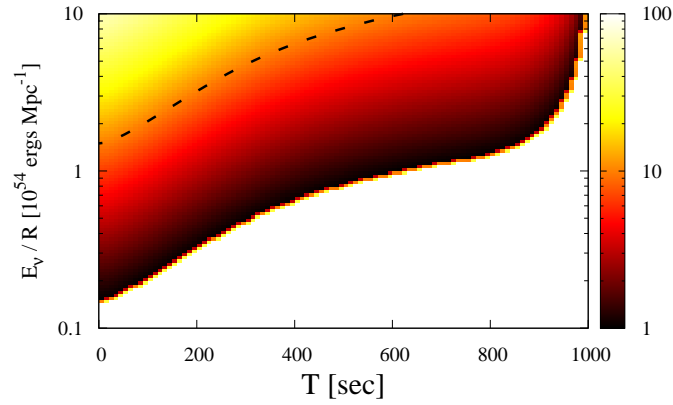


FIG. 5: SNRs of GW from NDAF for LISA. The white region in the right bottom part of the figure shows  $\text{SNR} \leq 1$ . The dashed line corresponds to  $\text{SNR} = 10$ .

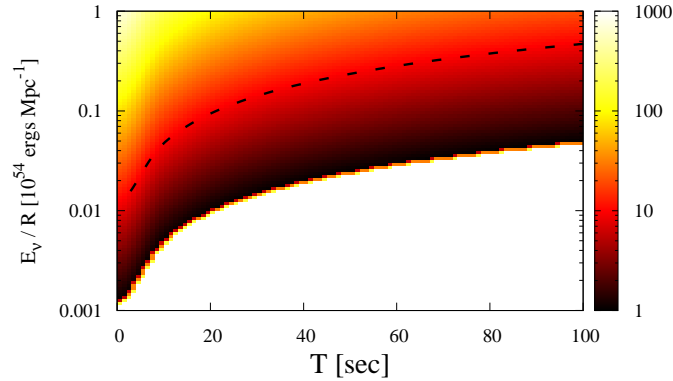


FIG. 6: Same as Figure 5, but for DECIGO/BBO.



## B. Multiple bursts

In this subsection, we consider the case of multiple bursts in order to take into account the intermittent time variability of the central engine. We employ the following time evolution for the neutrino luminosity,

$$L_\nu(t) = \sum_{i=1}^N \frac{E_\nu}{N\delta t} \Theta\left(t - \frac{i}{N}T\right) \Theta\left(\frac{i}{N}T + \delta t - t\right), \quad (22)$$

where  $N$  is the number of subbursts and  $\delta t$  is the duration of one subburst. We assume  $\delta t$  to be constant for any subburst. The total duration is  $T + \delta T \sim T$ , since we consider the case of  $\delta T \ll T$  [73]. Then, one finds the characteristic strain as

$$h_c(f) = \frac{\sqrt{\beta}h_\infty}{\pi^2 N \delta t f} \left| \frac{\sin(\pi \delta t f) \sin(\pi T f)}{\sin(\pi T f / N)} \right|. \quad (23)$$

Figure 7 shows the GW spectrum of Eqs. (21) and (23). The red solid line represents the single burst case, which is the same one as the green dashed line of figure 4. The green dashed line in this figure shows the case of multiple bursts with  $\delta t = 0.005$  s and  $N = 200$ . Both of the spectra are shown for  $T = 10$  s. We can see that those two spectra are different in the high-frequency range because multiple bursts are caused by many bursts with the shorter time scale. On the other hand, these spectra coincide with each other in the low-frequency range because the long-term behavior is independent from the detail of the burst. The difference typically appears only above  $f \sim N/T \sim 20$  Hz. Noting that the most sensitive frequency of LISA is about 1 mHz, we see that the detectability by LISA (and DECIGO/BBO) depends mainly  $E_\nu$  and  $D$ , so that the results of low-frequency GWs described in the previous subsection are unaltered even if a time variation is considered. By contrast, the detectability by advanced-LIGO is affected by fluctuations with short timescales. The SNR for advanced-LIGO calculated by Eq. (19) is  $\text{SNR} \sim 9(E_\nu/10^{54}\text{erg})(D/1\text{Mpc})^{-1}$  for  $\delta t = 0.005$  s and  $N = 200$ , which is about 100 times larger than that for the single burst case. As a result, the GW might be detectable by advanced-LIGO depending on the time properties of short-term variations during the burst. This implies that it may be possible not only to detect GWs by the burst memory, but also to extract important information about the temporal behavior of the central engine through GWs.

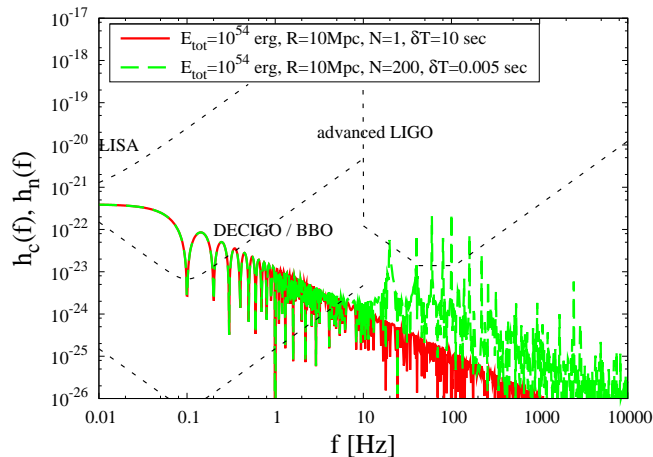


FIG. 7: GW spectra of a single burst (red solid line) and multiple bursts (green dashed line) from NDAF.

## C. Can we identify NDAF as a gravitational wave source?

Clearly, it is very important to identify sources emitting GWs in order to probe the central engine of GRBs and HNe. However, when we expect strong GW emission, prompt (electromagnetic) emission may be off-axis emission which is significantly diminished compared to on-axis emission. When the jet angle  $\theta_j$  is small enough compared to the viewing angle  $\xi$ , the peak flux scales as  $(\varepsilon F_\varepsilon)_{\text{max}} \propto [1 - (V/c) \cos(\xi - \theta_j)]^{-7/2}$ , where  $V$  is the velocity of the jet [46]. Then, the peak flux of the off-axis emission is very roughly estimated as  $(\varepsilon F_\varepsilon)_{\text{max}} \sim 10^{-7} \text{ ergs cm}^{-2} \text{ s}^{-1} L_{\gamma_{\text{max},51.5}}^{\text{iso}} (D/10\text{Mpc})^{-2}$

for  $\xi \sim \pi/4$  and  $\theta_j \sim 0.1$ , where  $L_{\gamma_{\max,51.5}}^{\text{iso}}$  is the luminosity around peak energy (Throughout this subsection we define  $Q_\alpha = Q/10^\alpha$  for a quantity  $Q$  in cgs unit). Although the details of the spectra and light curves depend on the jet structure, viewing angle and so on [46, 47], they may be detected by the BAT on *Swift* or the GBM on *Fermi*, if a bright GRB occurs within 10 Mpc. However, we may also keep in mind that many of the discovered nearby GRBs are dimmer than classical high-luminosity GRBs [48, 49]. For example, if the luminosity of such a low-luminosity GRB (for on-axis observers) is dimmer than that of a high-luminosity GRB by more than three orders of magnitude, and if the jet is well collimated [74], it may be difficult to detect prompt emission even for very nearby GRBs.

If we can detect both of the GW and prompt emission, we may infer the distance to the source by follow-up observations [75], and then we can obtain some important information on the energy budget of the central engine such as  $E_\nu$  and the efficiency of energy deposition from  $E_\gamma$ . Although we may expect detectable prompt X or gamma rays from such nearby GRBs whose GW signals are detectable, we can think of a different possibility, that GWs and neutrinos are expected, but no prompt photons. In the collapsar scenario, the jets have to penetrate the progenitor star to make the prompt emission. But, if they are choked inside the progenitor, we do not expect any prompt emission (which is called a failed GRBs) [50]. The possible population of such failed GRBs may not be neglected, as their local rate might be much higher than the rate of classical high-luminosity GRBs. Even in such cases, we may still expect detectable GW emission as long as the jets are launched by the neutrino-annihilation mechanism. In addition, coincident neutrino emission from NDAF should be expected, if GWs are caused by the neutrinos from NDAF. They may potentially help us to pin down the position of the bursts, and give us a clue whether GWs are caused by anisotropic neutrino emission (provided we know the distance). In figure 8, we plot detectabilities of 15-35 MeV neutrinos by the Super-Kamiokande (SK) and Mton detectors as well as the SNR of GW signals expected by LISA.  $P_1$  is the cumulative Poisson probability to detect at least one neutrino event,  $\sum_{n=1}^{\infty} (\mu^n e^{-\mu}/n!)$ , where  $\mu$  is an expected event number, and  $P_2$  is the cumulative Poisson probability to detect more than one neutrino event,  $\sum_{n=2}^{\infty} (\mu^n e^{-\mu}/n!)$ , in the 15-35 MeV range. Thick lines refer to Mton neutrino detectors, while thin lines refer to 22.5 kton neutrino detectors such as SK (see [51] for the case of core-collapse SNe). For simplicity, we have used a Fermi-Dirac distribution for neutrino spectra with a temperature of 3 MeV, assuming that the neutrino radiation energy is shared between electron and anti-electron neutrinos. As we can see, coincident neutrinos can also be detected. Especially, if we have Mton detectors, we should detect coincident neutrinos if the GW emission is caused by neutrinos, and possible detections of scattering events (rather than capturing events shown in the figure) become useful for positioning (see [52, 53] for the discussion of simultaneous observation of neutrino and GW in the case of core-collapse SNe).

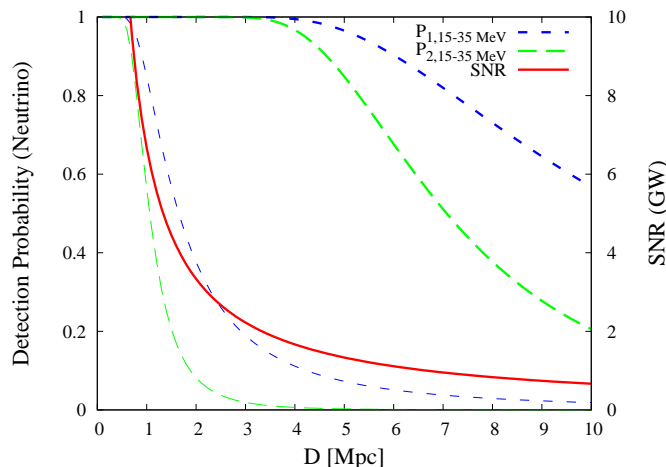


FIG. 8: The detection probability of neutrinos and SNR of GWs from NDAF. We assume  $E_\nu = 10^{54}$  ergs. See text for detail.

Later (follow-up) observations of photons seem to be crucially important to determine the distance to the source, as has been already mentioned. First, observations in the optical and radio bands may lead to discovering a HN (e.g., see [54]) associated with the formation of NDAF making jets. If GRB jets are successful and make prompt emission, possible detections of the prompt photons would be helpful for this purpose. In addition, it may also be possible to detect afterglow emission (which can be expected not only for successful GRBs, but also failed GRBs [55]). Whether the outflow is well collimated or not, it should be decelerated by colliding with the interstellar medium. When prompt emission is not observed, afterglows are called *orphan* afterglows. In this case, the afterglow is also dim in the early phase before the jet break, during which it may not be so easy to detect its emission. However, the expected flux after the time when  $\Gamma(t_p)\xi = 1$  does not depend on whether afterglows are orphan or not [55, 56]. Following the

external shock scenario [2], we can roughly estimate the peak flux after the peak time  $t_p \sim 8.1 \times 10^6 \text{ s} [5 + 2 \ln(10) + 2 \ln(\xi/\theta_{j,-1})](\xi/\theta_{j,-1})^2 \theta_{j,-1}^{8/3} (E_{\text{ej},53}^{\text{iso}})^{1/3} n^{-1/3}$ , as  $(\varepsilon F_\varepsilon)_{\text{max}} \sim 6 \times 10^{-9} \text{ ergs cm}^{-2} \text{ s}^{-1} \epsilon_{e,-1} E_{\text{ej},53}^{\text{iso}} (D/\text{Mpc})^{-2} t_7^{-2}$  for  $E_{\text{ej},53}^{\text{iso}} \sim 10^{53} \text{ ergs}$ ,  $\theta_j \sim 0.1$  and  $n \sim 1 \text{ cm}^{-3}$ , where  $\epsilon_e$  is the fraction of nonthermal electron energy,  $E_{\text{ej}}$  is the kinetic energy of the ejecta, and  $n$  is the density of interstellar medium [56], respectively. Although actual detectabilities depend on the detail of the afterglow spectra, this afterglow emission could be detected by groundbased optical telescopes and X-ray satellites such as *Swift*, future MAXI and EXIST. Since the spectra and light curves depend on  $\theta_j$  and  $\xi$ , their detection could potentially give us some information about relevant parameters such as  $\theta_j$  and  $\xi$ , leading to a crude estimate of the asphericity parameter  $a$  under our NDAF scenario. Those later observations (i.e., detecting an associated HN component, prompt and afterglow emissions), combined with GW and neutrino observations, may help us to reveal the central engine of GRBs and HNe.

#### IV. THE GRAVITATIONAL WAVE BACKGROUND

We are now in a position to discuss the contribution of GWs from NDAF of GRBs to the background GW radiation. According to Phinney [57], the sum of the energy densities radiated by a large number of independent GRBs at each redshift is given by the density parameter  $\Omega_{\text{GW}}(f) \equiv \rho_c^{-1} (d\rho_{\text{GW}}/d \log f)$  as

$$\Omega_{\text{GW}}(f) = \frac{1}{\rho_c c^2} \int_0^\infty dz \frac{R_{\text{GRB}}(z)}{1+z} \left| \frac{dt}{dz} \right| f_z \frac{dE_{\text{GW}}(fz)}{df}, \quad (24)$$

where  $\rho_c = 3H_0^2/(8\pi G)$  is the cosmic critical density,  $R_{\text{GRB}}(z)$  is the GRB rate per comoving volume, and  $f_z \equiv (1+z)f$ . The cosmological model enters with  $|dt/dz| = [(1+z)H(z)]^{-1}$  and, for a flat geometry,  $H(z) = H_0[\Omega_\Lambda + \Omega_M(1+z)^3]$ . We adopt the cosmological parameters  $\Omega_M = 0.3$ ,  $\Omega_\Lambda = 0.7$ , and  $H_0 = 100 h_0 \text{ km s}^{-1} \text{ Mpc}^{-1}$  with  $h_0 = 0.72$ . For the GRB rate, we employ the following GRB rate history (GRB3 model in Refs. [58, 59]) in units of  $\text{yr}^{-1} \text{ Gpc}^{-3}$ ,

$$R_{\text{GRB}} = R_0 \frac{46e^{3.4z}}{e^{3.8z} + 45} F(z, \Omega_m, \Omega_\Lambda), \quad (25)$$

where  $F(z, \Omega_m, \Omega_\Lambda) = \sqrt{\Omega_\Lambda + \Omega_m(1+z)^3}/(1+z)^{3/2}$ . Note that the dependence on the overall GRB rate history is so small that it is enough to use the above history for our purpose of demonstration.

In figure 9, the calculated  $\Omega_{\text{GW}}$  is plotted together with the sensitivity curves of future detectors. We assume that all GRBs have  $T = 10 \text{ sec}$  for simplicity. The red solid and green dashed lines are obtained for a GRB rate of  $R_0 = 18$  which is expected for high-luminosity GRBs, while the blue dotted line is with one for  $R_0 = 500$  which may be expected for low-luminosity GRBs. The red solid line is obtained with the single-burst spectrum (Eq. (21)), and the green dashed line is for the multiple-burst spectrum (Eq. (23)) so that these lines differ above 1 Hz. The blue dotted line is for the multiple burst spectrum. The enhancement of the GW background due to inclusion of time variation does not change the detectability by space-based interferometers since the most sensitive frequency is about 0.1 Hz.

Although we have used the inferred rates for successful GRBs, we may expect a larger contribution to the GW background if there is large population of failed GRBs. At present it is difficult to predict the rate of such choked jets, but we might expect that the rate of failed GRB is typically smaller than the SN Ibc rate. Then, the possible contribution to the GW background is at most  $\Omega_{\text{GW}} h_0^2 \lesssim 10^{-15}$  at  $\sim 0.01 - 0.1 \text{ Hz}$  (see [59, 60] for a discussion of the neutrino background from GRBs and HNe).

#### V. SUMMARY AND DISCUSSIONS

In this paper, we have calculated the amplitudes and spectra of GWs from gamma-ray bursts, which are expected in the neutrino-annihilation mechanism above an NDAF disk in the collapsar scenario. We show that GWs can be detected by LISA and DECIGO/BBO if the source distance is  $D \lesssim$  a few Mpc. The expected rates of high- and low-luminosity GRBs occurring at  $D < 10 \text{ Mpc}$ , which correspond to the rates of bursts that can be observed by  $\sim 5 \text{ Mton}$  neutrino detectors [52], are  $\sim 2 \times 10^{-5} \text{ yr}^{-1}$  and  $\sim 10^{-4} - 10^{-3} \text{ yr}^{-1}$ , respectively. Hence, detections of GW signals are possible only when GRBs fortunately occur in the nearby universe. Nevertheless, the possible GW signals are very important in the sense that they can probe the mechanism of the GRB central engine. Obtained GW spectra are *flat* at low frequencies, which is the characteristic feature of the GW memory effect. In order to detect GWs with LISA or DECIGO/BBO, sufficiently large values of the anisotropy parameter  $\alpha$  and large values of the released burst energy are typically required. Since the MHD mechanism may typically lead to a smaller burst

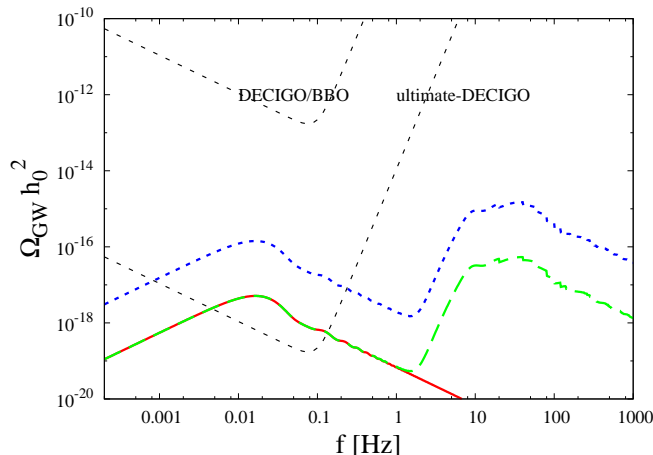


FIG. 9: The energy density parameter of gravitational wave background (GWB). See text for detail.

energy compared to the neutrino-annihilation mechanism (where  $E_\nu \sim 10^{53-54}$  ergs is needed), detections of flat GW spectra at low frequencies from extragalactic GRBs would allow us to infer that the central engine is governed by the neutrino-annihilation mechanism above an NDAF disk. We show that coincident neutrinos should be detected if we have Mton detectors as long as GWs arise from the neutrino emission, which should also give us important clues about the central engine (e.g., estimate of  $E_\nu$  allows us to make a consistency check for the burst energy triggering the GW emission).

In order to identify the source emitting GWs, later electromagnetic observations will be crucial. We may see prompt emission, afterglow emission and supernova emission. Although the former is significantly diminished when the viewing angle is very large, we may be able to detect it for very nearby bursts. Afterglow emission is also detectable even if we have orphan afterglows. Successful observations of GWs, neutrinos and photons will allow us to diagnose the central engine of GRBs and to obtain some clues on the jet production mechanism. In addition, we can expect that HNe are associated with GRBs (but it may not be necessarily the case). Detections of HNe in the optical and/or radio band will give us profound information about the explosion mechanism of HNe. Strong GW and neutrino emission can be expected since the neutrino-annihilation mechanism requires that the radiated neutrino energy is very large ( $E_\nu \sim 10^{53-54}$  ergs). On the other hand, it would be more difficult to expect detectable GW signals from the MHD mechanism. Hence, if we have very nearby GRBs, non-detections of both GWs and neutrinos might suggest the MHD mechanism rather than neutrino-annihilation which seems to have some caveats (e.g., the very strong dependence on the disk temperature and inefficiency in production of fireballs). Whether signals are detected or not, simultaneous observations by GWs and neutrinos will be important to probe the central engine of GRBs and HNe, even though the burst rate is not so large.

In this work, we have used a thin disk or an oblate spheroid model to mimic NDAF. Such a simplified treatment is sufficient for our purpose, and the characteristic feature in the low-frequency range will not be altered even if we employ elaborate numerical simulations. But, although sufficiently realistic calculations have not been done so far, further studies and developments may allow to evaluate both the neutrino flux and the GW amplitude more quantitatively. Also, the effect of neutrino oscillation, which is neglected in this work, should be included for more quantitative predictions. In addition, we have employed the fiducial energy emitted by neutrinos as  $E_\nu = 10^{54}$  ergs, which is also unknown. The assumptions employed for this value are that the energy of a GRB jet is  $E_j \sim 10^{52}$  ergs and the efficiency of energy conversion from neutrinos to a jet is 1% for the neutrino-annihilation mechanism. Since GRBs have a variety of energetics,  $E_\nu$  might be significantly larger or smaller than this value. Detections of GWs and neutrinos are useful since the signal-to-noise ratios of GW show a linear increase with  $E_\nu$ . In addition, we might have information about the efficiency of energy conversion, which is theoretically important, through obtaining the jet energy from electromagnetic observations.

Although we have mainly considered production of GRB jets with a duration of  $\sim 10-100$  s, required for explaining prompt emission, there are additional possibilities of the GW emission. Recent observations by *Swift* have shown that many GRBs have flares in the afterglow phase, which suggest that the central engine is active for a longer time than the duration of the prompt emission [61]. Flares are also likely to be energetic, and the radiation energy of some flares is even comparable to that of the prompt emission. Possibly, they may be produced by slower and less collimated jets, and their geometrically corrected energy may also be comparable to that of the prompt emission. Then, we could

also expect GW emission even in the early afterglow phase.

### Acknowledgments

We would like to thank H.-Th. Janka, K. Kotake, E. Müller, and N. Sago for stimulating discussion. This study was supported by the Japan Society for Promotion of Science (JSPS) Research Fellowships and the Grants-in-Aid for the Scientific Research from the Ministry of Education, Science and Culture of Japan (No. S19104006) and for the GCOE Program “The Next Generation of Physics, Spun from Universality and Emergence” from MEXT.

- 
- [1] T. Piran, *Reviews of Modern Physics* **76**, 1143 (2005).
  - [2] P. Meszaros, *Reports on Progress in Physics* **69**, 2259 (2006).
  - [3] D. A. Frail *et al.*, *Astrophys. J.* **562**, L55 (2001).
  - [4] J. S. Bloom, D. A. Frail, and S. R. Kulkarni, *Astrophys. J.* **594**, 674 (2003).
  - [5] G. Ghirlanda, G. Ghisellini, and D. Lazzati, *Astrophys. J.* **616**, 331 (2004).
  - [6] S. E. Woosley, *Astrophys. J.* **405**, 273 (1993).
  - [7] J. Hjorth *et al.*, *Nature (London)* **423**, 847 (2003).
  - [8] K. Z. Stanek *et al.*, *Astrophys. J.* **591**, L17 (2003).
  - [9] K. Iwamoto *et al.*, *Nature (London)* **395**, 672 (1998).
  - [10] S. E. Woosley and J. S. Bloom, *ARA&A* **44**, 507 (2006).
  - [11] B. Paczynski, *Astrophys. J.* **494**, L45 (1998).
  - [12] A. I. MacFadyen and S. E. Woosley, *Astrophys. J.* **524**, 262 (1999).
  - [13] R. Popham, S. E. Woosley, and C. Fryer, *Astrophys. J.* **518**, 356 (1999).
  - [14] T. Di Matteo, R. Perna, and R. Narayan, *Astrophys. J.* **579**, 706 (2002).
  - [15] K. Kohri and S. Mineshige, *Astrophys. J.* **577**, 311 (2002).
  - [16] W.-X. Chen and A. M. Beloborodov, *Astrophys. J.* **657**, 383 (2007).
  - [17] N. Kawanaka and S. Mineshige, *Astrophys. J.* **662**, 1156 (2007).
  - [18] R. Birkel, M. A. Aloy, H.-T. Janka, and E. Müller, *A&A* **463**, 51 (2007).
  - [19] K. Kohri, R. Narayan, and T. Piran, *Astrophys. J.* **629**, 341 (2005).
  - [20] M. Ruffert, H.-T. Janka, K. Takahashi, and G. Schaefer, *A&A* **319**, 122 (1997).
  - [21] D. Proga, A. I. MacFadyen, P. J. Armitage, and M. C. Begelman, *Astrophys. J.* **599**, L5 (2003).
  - [22] S. Nagataki, R. Takahashi, A. Mizuta, and T. Takiwaki, *Astrophys. J.* **659**, 512 (2007).
  - [23] R. D. Blandford and R. L. Znajek, *MNRAS* **179**, 433 (1977).
  - [24] Y. Mizuno, S. Yamada, S. Koide, and K. Shibata, *Astrophys. J.* **615**, 389 (2004).
  - [25] J. C. McKinney and C. F. Gammie, *Astrophys. J.* **611**, 977 (2004).
  - [26] M. V. Barkov and S. S. Komissarov, *MNRAS* **385**, L28 (2008).
  - [27] V. V. Usov, *Nature (London)* **357**, 472 (1992).
  - [28] T. A. Thompson, P. Chang, and E. Quataert, *Astrophys. J.* **611**, 380 (2004).
  - [29] S. S. Komissarov and M. V. Barkov, *MNRAS* **382**, 1029 (2007).
  - [30] T. Takiwaki, K. Kotake, and K. Sato, *Astrophys. J.* **691**, 1360 (2009).
  - [31] L. Dessart, A. Burrows, E. Livne, and C. D. Ott, *Astrophys. J.* **673**, L43 (2008).
  - [32] N. Sago, K. Ioka, T. Nakamura, and R. Yamazaki, *Phys. Rev. D* **70**, 104012 (2004).
  - [33] T. Hiramatsu, K. Kotake, H. Kudoh, and A. Taruya, *MNRAS* **364**, 1063 (2005).
  - [34] A. Burrows and J. Hayes, *Phys. Rev. Lett.* **76**, 352 (1996).
  - [35] E. Müller and H.-T. Janka, *A&A* **317**, 140 (1997).
  - [36] E. Müller *et al.*, *Astrophys. J.* **603**, 221 (2004).
  - [37] C. D. Ott, A. Burrows, L. Dessart, and E. Livne, *Phys. Rev. Lett.* **96**, 201102 (2006).
  - [38] K. Kotake, N. Ohnishi, and S. Yamada, *Astrophys. J.* **655**, 406 (2007).
  - [39] Y. Suwa, T. Takiwaki, K. Kotake, and K. Sato, *Astrophys. J.* **665**, L43 (2007).
  - [40] C. D. Ott, *Classical and Quantum Gravity* **26**, 063001 (2009).
  - [41] K. Kotake, K. Sato, and K. Takahashi, *Rep. Prog. Phys.* **69**, 971 (2006).
  - [42] R. Epstein, *Astrophys. J.* **223**, 1037 (1978).
  - [43] É. É. Flanagan and S. A. Hughes, *Phys. Rev. D* **57**, 4535 (1998).
  - [44] M. S. Turner, *Nature (London)* **274**, 565 (1978).
  - [45] K. S. Thorne, *Phys. Rev. D* **45**, 520 (1992).
  - [46] R. Yamazaki, K. Ioka, and T. Nakamura, *Astrophys. J.* **571**, L31 (2002).
  - [47] J. Granot, A. Panaitescu, P. Kumar, and S. E. Woosley, *Astrophys. J.* **570**, L61 (2002).
  - [48] E.-W. Liang, B.-B. Zhang, and B. Zhang, *Astrophys. J.* **670**, 565 (2007).
  - [49] D. Guetta and T. Piran, *Journal of Cosmology and Astro-Particle Physics* **7**, 3 (2007).

- [50] P. Mészáros and E. Waxman, Physical Review Letters **87**, 171102 (2001).
- [51] S. Ando, J. F. Beacom, and H. Yüksel, Physical Review Letters **95**, 171101 (2005).
- [52] Kistler, M. D., Yüksel, H., Ando, S., Beacom, J. F., & Suzuki, Y. 2008, arXiv:0810.1959
- [53] G. Pagliaroli, F. Vissani, E. Coccia, and W. Fulgione, Physical Review Letters **103**, 031102 (2009).
- [54] A. M. Soderberg, E. Nakar, E. Berger, and S. R. Kulkarni, Astrophys. J. **638**, 930 (2006).
- [55] Y. F. Huang, Z. G. Dai, and T. Lu, MNRAS **332**, 735 (2002).
- [56] T. Totani and A. Panaitescu, Astrophys. J. **576**, 120 (2002).
- [57] E. S. Phinney, astro-ph/0108028 (2001).
- [58] C. Porciani and P. Madau, Astrophys. J. **548**, 522 (2001).
- [59] K. Murase, Phys. Rev. D **76**, 123001 (2007).
- [60] S. Nagataki, K. Kohri, S. Ando, and K. Sato, Astroparticle Physics **18**, 551 (2003).
- [61] A. D. Falcone *et al.*, Astrophys. J. **671**, 1921 (2007).
- [62] V. B. Braginskii and K. S. Thorne, Nature (London) **327**, 123 (1987).
- [63] M. Obergaulinger, M. A. Aloy, and E. Müller, A&A **450**, 1107 (2006).
- [64] M. Shibata, Y. T. Liu, S. L. Shapiro, and B. C. Stephens, Phys. Rev. D **74**, 104026 (2006).
- [65] L. S. Finn and K. S. Thorne, Phys. Rev. D **62**, 124021 (2000).
- [66] N. Seto, S. Kawamura, and T. Nakamura, Phys. Rev. Lett. **87**, 221103 (2001).
- [67] A. M. Soderberg *et al.*, Nature (London) **442**, 1014 (2006).
- [68] This is called *burst with memory* [62]. This nature can be directly seen in the time integral in Eq. (7). Largely-aspherical mass ejection and magnetic fields can lead to a similar GW memory [63, 64]. The detectability of such GW bursts with memory was discussed in [45].
- [69] The geometrically corrected gamma-ray energy is smaller by one order of magnitude,  $E_\gamma \sim 10^{51}$  ergs. But note that only the fraction of the jet energy is converted into the radiation energy. For example, in the internal shock model, a fraction of the jet kinetic energy  $\epsilon_{\text{int}} \lesssim 0.6$  can be converted into the internal energy, and a fraction of the internal energy is used for acceleration of nonthermal electrons (and amplification of the magnetic field). Such large jet energy will also be required in some more specific scenarios. For instance, the hypothesis that GRBs are the sources of ultra-high-energy cosmic rays is typically require  $E_j \gtrsim 10^{52}$  ergs.
- [70] It should be noted that both  $\alpha$  and  $\beta$  depend on  $dL_\nu/d\Omega$  so that the configuration of neutrino emission is required in order to estimate more precise energy of GW. This is different from ordinary quadrupole formula, in which the total energy can be calculated just by the time derivative of quadrupole wave amplitude  $A_{lm}^{E2}$  and  $A_{lm}^{B2}$ . See §III in Müller and Janka [35] for detail.
- [71] For another example, flares have been observed in many GRBs and they are usually attributed to the long time activity of the central engine.
- [72] The noise curve of advanced LIGO is taken from [43]. As for LISA and DECIGO/BBO, we adopt  $S_h(f) = 1.22 \times 10^{-51} f^{-4} + 2.11 \times 10^{-41} + 1.22 \times 10^{-37} f^2$  [65] and  $S_h(f) = 4.5 \times 10^{-51} f^{-4} + 4.5 \times 10^{-45} f^2$  [66], in which  $f$  is measured in unit of Hz, respectively.
- [73] Generally speaking, this  $\delta t$  may not correspond to the observed duration of one subburst. This is because the latter can be rather determined by other time scales such as the angular spreading time (which becomes important when photons are radiated). Note that, if  $\delta t \sim T/N$ , the difference between the two case is diminished.
- [74] It was suggested that the outflow of GRB 060218 may not be well collimated [48, 49, 67].
- [75] It seems difficult to identify the position of the source only with GW observations only, even if we have two or three GW observatories in the future.